One Earth

Article

Six Decades of Glacier Mass Changes around Mt. Everest Are Revealed by Historical and Contemporary Images

Graphical Abstract

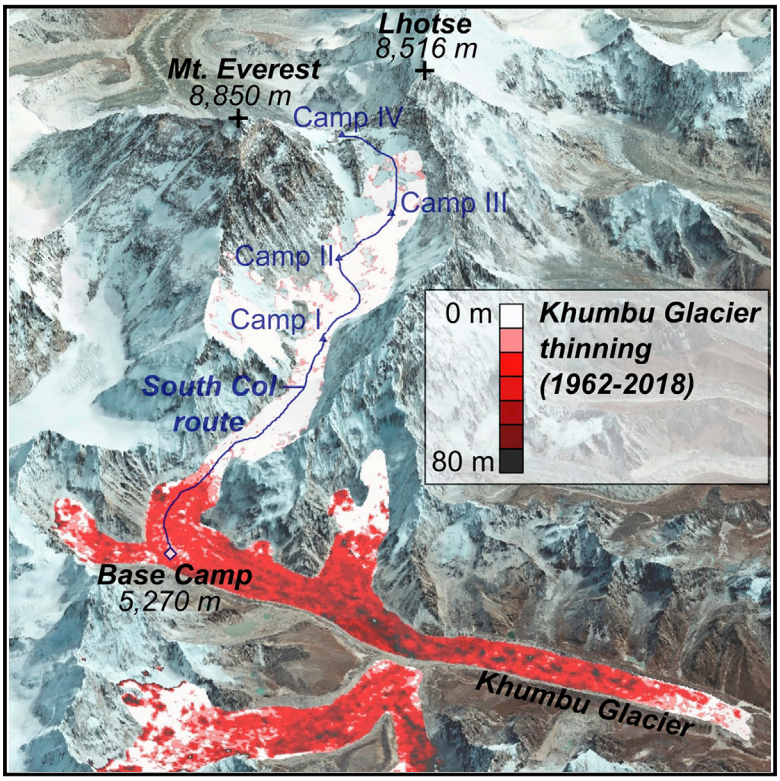

Highlights

- Glaciers around Mt. Everest have thinned by more than 100 m since the 1960s
- The rate of ice mass loss has consistently accelerated over the past six decades
- Glacier thinning has occurred at above 6,000 masl
- Surge-type glacier behavior has been identified for the first time in the region

Authors

Owen King, Atanu Bhattacharya, Sajid Ghuffar, Alex Tait, Sam Guilford, Aurora C. Elmore, Tobias Bolch

Correspondence

ogak1@st-andrews.ac.uk

In Brief

We generated the longest possible time series of glacier elevation-change measurements from satellite image archives to show how glaciers around Mt. Everest have reacted to climatic change since the 1960s. The rate of ice loss in the region has consistently increased over the last six decades, and ice loss is now occurring at extreme altitudes. Accurate, long-term measurements of ice-loss rates are vital if we are to understand the impact of glacier recession on local and regional hydrology.

King et al., 2020, One Earth 3, 608–620
November 20, 2020
https://doi.org/10.1016/j.oneear.2020.10.019

CellPress

CellPress
OPEN ACCESS

Gold Standard for the Global Goals
1 ton of CO_2 offset

One Earth

Article

Six Decades of Glacier Mass Changes around Mt. Everest Are Revealed by Historical and Contemporary Images

Owen King,[1,4,*] Atanu Bhattacharya,[1] Sajid Ghuffar,[1,2] Alex Tait,[3] Sam Guilford,[3] Aurora C. Elmore,[3] and Tobias Bolch[1]
[1]School of Geography and Sustainable Development, University of St Andrews, St Andrews, Scotland, UK
[2]Department of Space Science, Institute of Space Technology, Islamabad
[3]National Geographic Society, Washington, DC, USA
[4]Lead Contact
*Correspondence: ogak1@st-andrews.ac.uk
https://doi.org/10.1016/j.oneear.2020.10.019

SCIENCE FOR SOCIETY Meltwater from Himalayan glaciers sustains the flow of rivers that are heavily depended on by downstream communities across the densely populated region of Southeast Asia. Himalayan glaciers are shrinking in response to a changing climate, and measurements of glacier mass loss are vital for the calibration of models used for predicting the future variability of meltwater runoff. Here, we produced the longest possible time series of glacier mass-change measurements from satellite archives and found that the rate of ice loss from glaciers close to Mt. Everest has consistently increased since the early 1960s. We show how glacial lakes in the region have amplified ice loss and illustrate how ice loss has begun to occur at extreme altitudes, where large volumes of ice that were formerly less susceptible to melt are stored. The rate of ice loss across the Himalaya is likely to increase in the coming decades in response to further warming, which could be amplified at high altitude.

SUMMARY

The accurate quantification of current and past Himalayan glacier mass budgets is vital if we are to understand the evolution of the Asian water tower, which provides water to the planet's most populous region. In this work, we generated a geodetic time series spanning six decades over 79 glaciers surrounding Mt. Everest and found consistent acceleration of glacier mass loss between the 1960s (-0.23 ± 0.12 mwe a^{-1}) and the modern era (-0.38 ± 0.11 mwe a^{-1} from 2009 to 2018). Glacier mass loss has varied depending on glacier terminus type and surface characteristics, and glacier thinning is now occurring at extreme altitudes (>6,000 masl). Our time series also captures the first documented surge of a glacier in the Mt. Everest region. These multi-decadal observations of glacier mass loss form a baseline dataset against which physically based glacier evolution models could be calibrated before they are used for predicting future meltwater yield.

INTRODUCTION

Glacier meltwater originating from the Hindu Kush Himalaya sustains the flow of some of south Asia's largest rivers, on which more than 230 million people living in the mountains and hills of the region and, to a lesser extent, people living in the lowlands depend for their water supply.[1,2] In the face of climate change, the contribution of these glaciers to river flow will become increasingly important as drought intensity and duration increase in the coming decades.[3–5] However, glaciers in the Himalaya are shrinking,[6] and their contribution to downstream river flow will become unsustainable in the future.[7,8] The accurate quantification of the current and historical rate of glacier melt is vital if the timing and magnitude of future meltwater yield are to be constrained by the projections of glacier evolution models.

The mass loss of individual glaciers can be monitored by field measurements of glacier accumulation and ablation, the difference between which determines a glacier's mass balance.[9,10] *In situ* measurements of glacier mass balance take place at a few benchmark glaciers across high-mountain Asia (HMA),[6,11] but such measurements are logistically difficult, and the application of this method is not possible at a regional scale. The use of laser altimetry data, interferometric synthetic aperture radar (InSAR) data, and stereo satellite imagery to generate digital elevation models (DEMs), which can be analyzed to derive the rates of glacier surface elevation change, is therefore the most practical way to examine geodetic glacier mass balance over

broad regions.[12,13] Remote-sensing studies of glacier surface elevation change have been conducted across the Himalaya.[6] The most comprehensive information on rates of glacier mass loss in the Himalaya since 2000 is provided by Shean et al.[14] Glaciers in the eastern Himalaya have lost ice at the fastest rate over the last two decades, but glaciers in the central and western Himalaya also show more ice loss than elsewhere in HMA.[14] Recent studies have teamed declassified Hexagon KH-9 spy satellite imagery with modern satellite data to show that regional patterns of ice mass loss have persisted for several decades and also that rates of ice loss have increased since the early 1970s.[6,15–17] Although large-scale studies have undoubtedly provided valuable insights into the overall behavior of Himalayan glaciers, the analyses of ice-loss data over broad regional and temporal scales could mask substantial variability and the associated drivers of exacerbated, or diminished, glacier recession. The incorporation of high-resolution (~2–8 m) Corona KH-4 spy satellite data, alongside Hexagon KH-9 images and contemporary (post-2000) satellite data, presents the opportunity to study glacier change in improved detail at a sub-regional level across several decades. The suitability of stereo Corona KH-4 data for generating DEMs for the study of glacier surface elevation change has been shown by Bolch et al.[18] More recently, Mukherjee et al.[19] combined Corona KH-4 data from 1971 with the shuttle radar topographic mission (SRTM) DEM and Cartosat imagery to highlight an increased rate of glacier mass loss in Lahaul-Spiti (western Himalaya) since around 2000.

The potential for the detailed long-term study of glacier behavior is perhaps greater in the Mt. Everest region than elsewhere in the Himalaya, mainly because of the need for accurate topographic information to aid early mountaineering expeditions. The topography of Mt. Everest, also known by its official names of Sagarmatha and Qomolangma in Nepal and China, respectively, and its surrounding valleys have been surveyed repeatedly by a variety of methods since the mid-1920s, and glacier extent has been recorded at numerous points prior to the modern satellite era, although not all of these early surveys are suited to quantifying glacier change. The 1955 photographic surveys and associated topographic map of Erwin Schneider provide the earliest region-wide record of glacier extent around Mt. Everest. The Schneider Alpine Club map is based on extensive field survey data on the southern (Nepali) side of the main orographic divide, which was complemented with later aerial photography to cover the wider area.[20] The multi-temporal nature of the source data of the Schneider map inhibits its use for the derivation of accurate rates of glacier surface elevation change, but it provides an important snapshot of glacier conditions before the declassified satellite imagery era. In 1984, National Geographic conducted an airborne photographic survey of the Mt. Everest region, including glaciers flowing north of Mt. Everest onto the Tibetan Plateau, by using a Wild RC-10 camera.[21] In 1992, the Survey Department of Nepal conducted another aerial photography survey of the country by using a Wild RC-30 camera.[22] Some studies have combined DEMs generated from declassified data, the mentioned aerial imagery, or topographic maps with contemporary imagery over a subset area to examine glacier change over broad periods.[18,23,24] Other studies have examined glacier change at the regional scale,[15,25,26] but their use of contemporary optical imagery or InSAR data limited their study period to the post-2000 era. So far, no one study has combined the various sources of geodetic data covering Mt. Everest to study glacier change at decadal time steps over the wider region.

In this work, we significantly extend the work by Bolch et al.[18,27] to produce the longest possible geodetic time series of glacier surface elevation change in the Everest region on both the north and south sides of the main orographic divide and glaciers to the east of Mt. Everest. We have compiled geodetic datasets derived from declassified Corona KH-4 (1962), Corona KH-4B (1969), and Hexagon KH-9 (1976) imagery, aerial photographic surveys (1984 and 1992), and satellite imagery acquired by the Advanced Spaceborne Thermal Emission and Reflection Radiometer (ASTER; 2001), Cartosat (2009 and 2018), and PlanetScope (2017) sensors over the regional extent of the National Geographic survey from 1984 (Figures 1 and 2), which we slightly extend to cover glacier extent fully (e.g., Kangshung and Barun Glaciers). We complement this time series with data from a 2019 high-resolution light detection and ranging (LiDAR) survey of the Khumbu Glacier, including the Western Cwm,[28] to examine high-altitude glacier change, where surface conditions often hinder medium-resolution remotely sensed data. We also used the modeled ice-thickness data[29] to compare the distribution of thinning through the elevation range of Mt. Everest's glaciers with their altitudinal distribution of ice volume. To compare ice-loss rates in the region with those elsewhere in the Himalaya (Figure S1 and Table S1), we converted glacier surface elevation change to ice-mass change in order to derive estimates of geodetic glacier mass balance. Our region of study for the time series of DEMs covers 212 glaciers with a total area of 419 km^2 (in 2018) ranging from 4,750 to >8,000 masl (Figure 1). We derived ice-loss estimates for 79 (>1 km^2) of these glaciers (369 km^2 [88% of glacier area]) and describe the methodology in detail in the Experimental Procedures.

Using these data, we examine the rate of ice loss over nearly 60 years across seven quasi-decadal time steps. We highlight sources of variability in rates of glacier mass loss, namely the presence of glacier debris mantles or proglacial lakes and the influence of topography and glacier hypsometry on glacier thinning. We also provide evidence of surge behavior of a glacier close to Mt. Everest, which has not been documented elsewhere. This time series of mass-balance estimates provides a benchmark of unprecedented detail against which physically based models of glacier evolution can be calibrated to predict future glacier behavior and meltwater yield.

RESULTS

Glacier Surface Elevation Change around Mt. Everest

Over our study period, the heavy debris cover on the surface of the ablation zone of most of the Mt. Everest region's largest glaciers prevented the substantial retreat of glacier termini, aside from those glaciers that have developed large proglacial lakes (Figure 2) and clean-ice glaciers to the north of the main orographic divide. Glacier area in our study area was 440 ± 10 km^2 in 1962 versus 419 ± 4 km^2 in 2018. However, the differencing of DEMs in our time series reveals considerable glacier surface lowering, and thereby glacier thinning, across the Mt. Everest region over the last six decades (Figure 3). Substantial

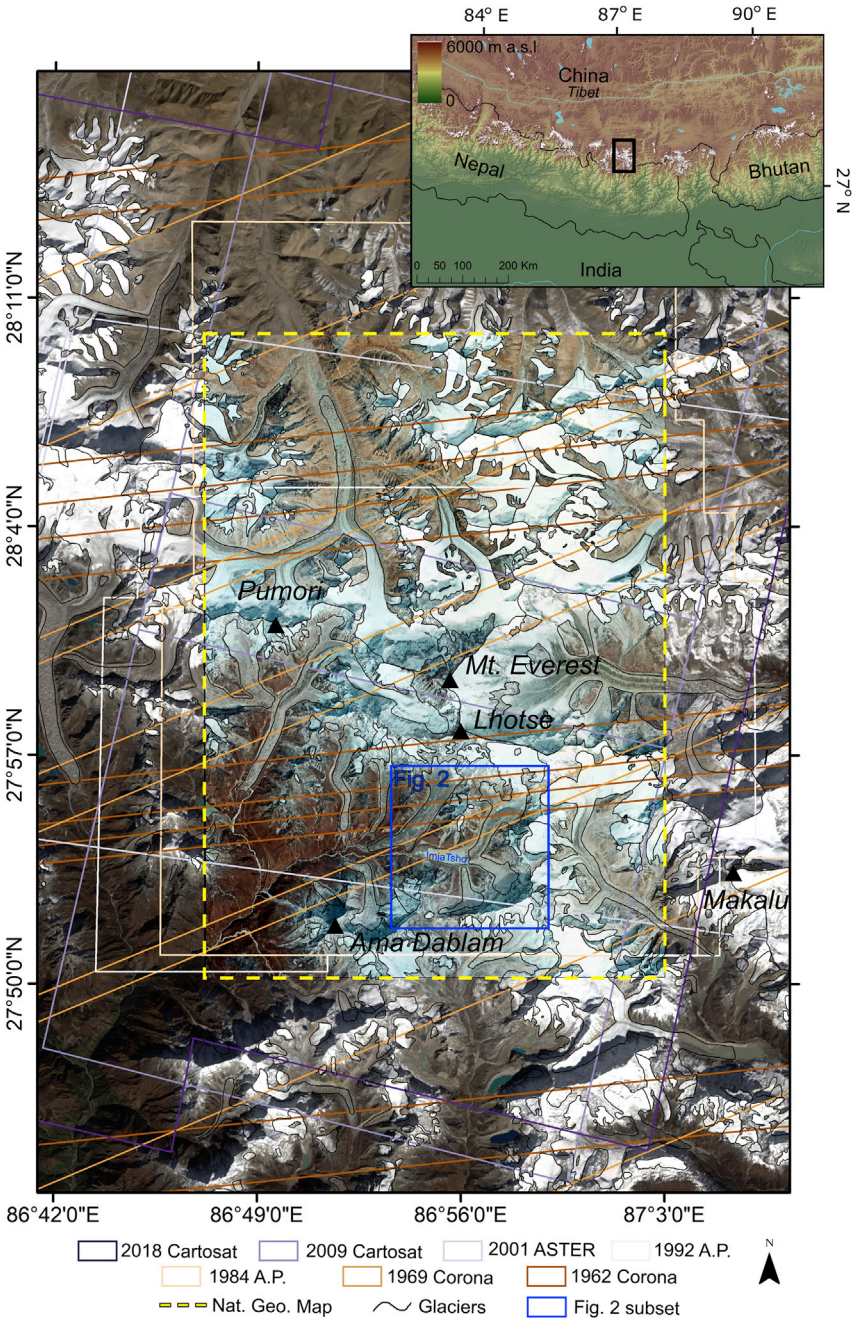

Figure 1. The Glacial Setting of the Mt. Everest Region

The extent of the 1984 National Geographic map is covered by the higher-resolution WorldView imagery, and the wider region is covered by a Landsat OLI scene from 2015. A.P. refers to aerial photography, and Imja Tsho (the focus area for Figure 2) is marked by the blue box. Glacier extent is modified from the Randolph Glacier Inventory (RGI) V6.0.[30]

thinning is evident across each glacier within our study area over the full study period regardless of size, aspect, surface cover type, or elevation range. The greatest ice losses have occurred from Barun Glacier, Rongbuk East Glacier, and Lhotse Shar and Imja Glaciers (which merge to form one ice body and are hereafter referred to as Lhotse Shar/Imja Glacier). The differencing of DEMs shows that individual parts of each of these glaciers have thinned by >100 m between 1962 and 2018. Barun Glacier thinned by an exceptional 150 m between 1962 and 2018 in its central ablation zone. The lake-terminating Lhotse Shar/Imja Glacier and clean-ice Rongbuk East Glacier thinned most at their termini. The region-wide mean rate of glacier surface elevation change over the full study period (1962–2018) was -0.39 ± 0.13 m a^{-1}.

The rate of surface elevation change has increased over glacier surfaces toward the present day (Figure 3). We calculated the mean rate of elevation change over the full extent of individual glaciers, took a region-wide mean of those values, and determined that between 1962 and 1969, glacier surfaces lowered at a mean rate of -0.28 ± 0.15 m a^{-1}. This rate increased to a mean of -0.41 ± 0.18 m a^{-1} between 1984 and 2000, and from 2009 to 2018 the mean rate was -0.52 ± 0.15 m a^{-1}. Glacier thinning varied spatially as well as temporally. The maximum thinning rate (-2.12 ± 0.09 m a^{-1}) occurred over the termini of lake-terminating glaciers between 2009 and 2018 (Figure 4E). The minimum rate of thinning over glacier ablation zones occurred at the termini of heavily debris-covered, land-terminating glaciers (e.g., Khumbu Glacier; Figure 4B). Thinning rates of ~1 m a^{-1} were widespread around the termini of clean-ice glaciers and in the middle reaches of debris-covered glacier ablation zones (Figures 4A and 4B).

The difference in surface elevation between the 2019 LiDAR DEM of Khumbu Glacier[30] and the 1984 DEM derived from aerial photographs shows that thinning (10–15 m) has occurred at elevations of up to 5,700 m on the southern side of the main orographic divide (Figure 5B). The thinning within the narrow trunk of the Khumbu icefall and at its broad base has occurred despite the high ice flux from the Western Cwm,[31] which is located above 6,000 masl. On the northern side of the main orographic divide, the difference in surface elevation between the 1984 DEM and 2018 Cartosat DEM suggests that a similar magnitude of thinning has occurred at up to 5,900 m in the main tributaries of Rongbuk Glacier and up to 6,300 masl on Rongbuk East Glacier (Figure 5A). The highest thinning rate we measured over land-terminating glaciers occurred at slightly lower elevations (5,300–5,500 masl). However, according to modeled estimates of glacier thickness[29] (Figure 4), which offer a good impression of the profile of distributed ice thickness but are subject to substantial

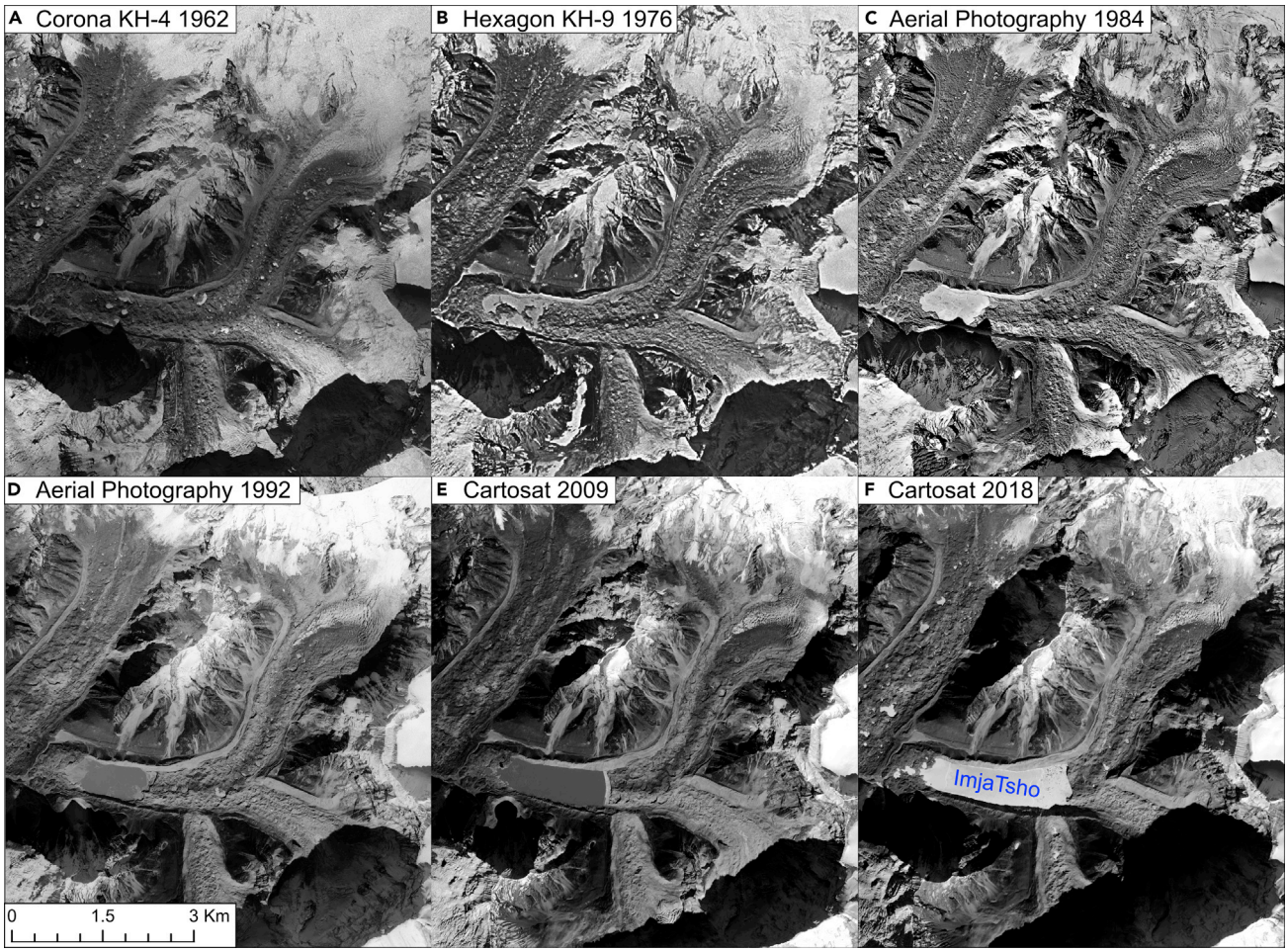

Figure 2. Evolution of Lhotse Shar/Imja Glacier and Imja Tsho from 1962 to 2018
Example orthoimages covering Lhotse Shar/Imja Glacier and Imja Tsho Lake from the different image sources.

uncertainties, particularly over debris-covered glaciers,[32] ~55% of the total glacier volume is situated above 5,700 masl in the Mt. Everest region. Contemporary thinning therefore continues to expand into an elevation range where a large amount of ice is stored (Figure 4).

A single example of glacier surface elevation gain is evident in our elevation-change datasets covering the periods 1962–1969, 1969–1976, 1976–1984, and 1984–2001 (Figure 6). Glacier RGI60-15.09839, which we refer to as Kangchungtse Glacier because of its situation beneath Kangchungtse (7,678 masl), showed surface elevation gain (~20 m) in the lower reaches of its wide accumulation zone (Figure 6A) and around its terminal position in the late 1960s and early 1970s (up to 40 m) (Figure 6D). Between 1976 and 1984, this elevation gain became focused around the terminus of the glacier, which advanced ~400 m over the same period (Figure 6B). At the same time, the surface of the broad accumulation zone lowered (~20 m). The thickening at lower elevations (up to 90 m) and the advance (850 m) of the glacier were most pronounced between 1984 and 1992 and from 1992 to 2001 (Figure 6D), when an extensive network of crevasses developed throughout the debris-covered portion of the glacier tongue (Figure S2). Glacier surface velocities, extracted from the ITS_LIVE dataset,[33,34] show that enhanced ice flow occurred in two zones along the glacier as it advanced (Figure 6D). In 1988, surface velocities of ~40 m a^{-1} were evident where the glacier narrows from its broad accumulation zone toward its tongue and were approximately twice as high as the flow rate measured in this part of the glacier when the advance ceased (in 2002). Between 1989 and 2001, ice surface velocities subsided higher up the glacier but increased within ~2 km of the glacier's terminus (Figure 6D). Maximum flow rates reached 30 m a^{-1} here in 1999, six times the rate of flow measured once the surge had ended in the same area of the glacier. After 2001, slight (~25 m) elevation gain was evident within ~250 m of the glacier's terminus, but most of the glacier's 4.5-km-long tongue thinned slightly (~15 m). Terminus proximal flow rates were <10 m a^{-1}, similar to those measured in 1988. There is little evidence of pervasive ice buildup in the glacier's broad accumulation zone in our data since 2001.

Geodetic Glacier Mass Balance

Akin to the changes in surface elevation, glaciers around Mt. Everest showed persistent and accelerating loss of ice mass since the 1960s. Between 1962 and 1969, the mean mass

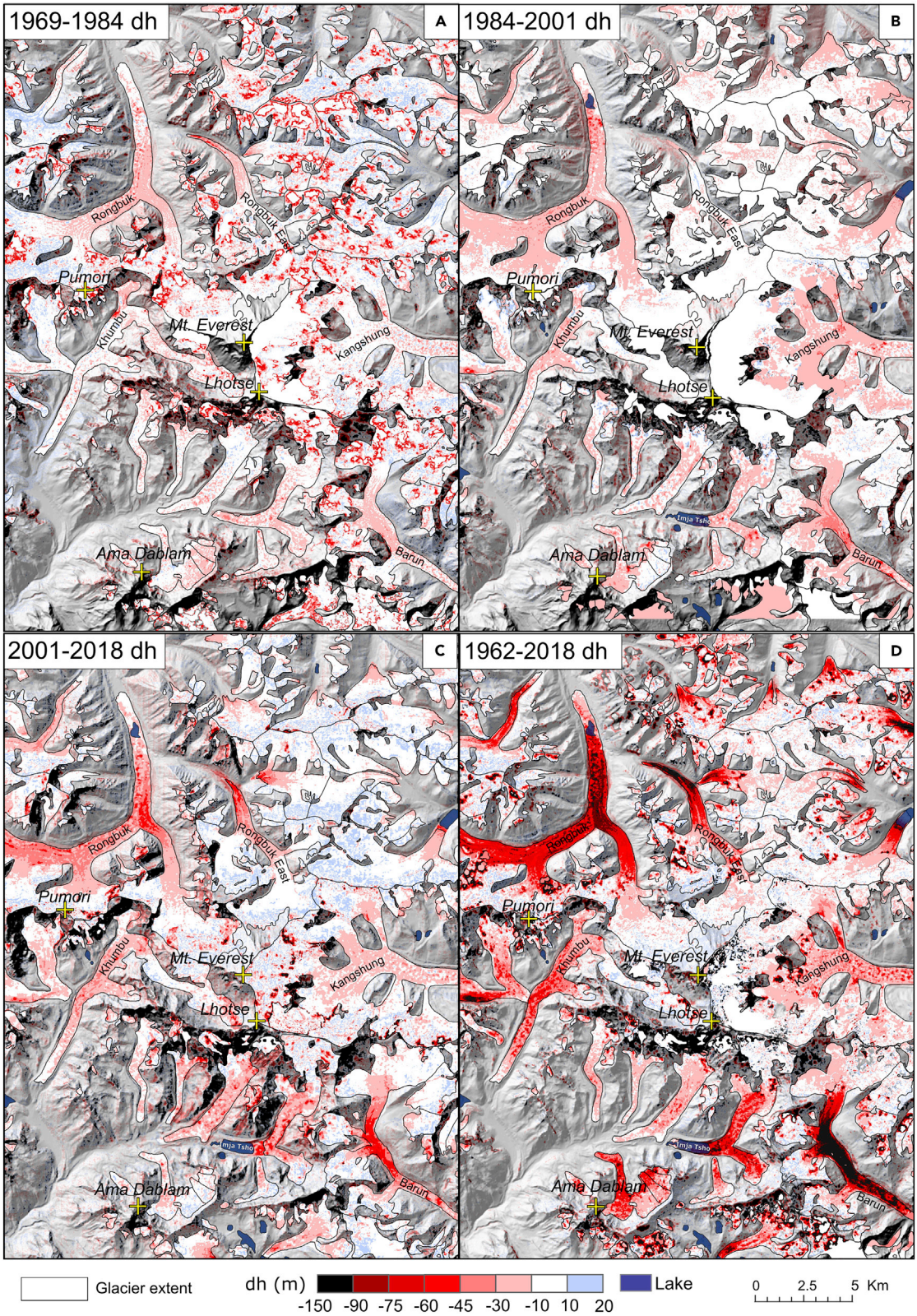

Figure 3. Glacier Surface Elevation Change (dh) in the Mt. Everest Region over Different Time Periods over the Extent of the 1984 National Geographic Map

1969–1984 (A), 1984–2001 (B), 2000–2018 (C), and the entire study period, 1962–2018 (D).

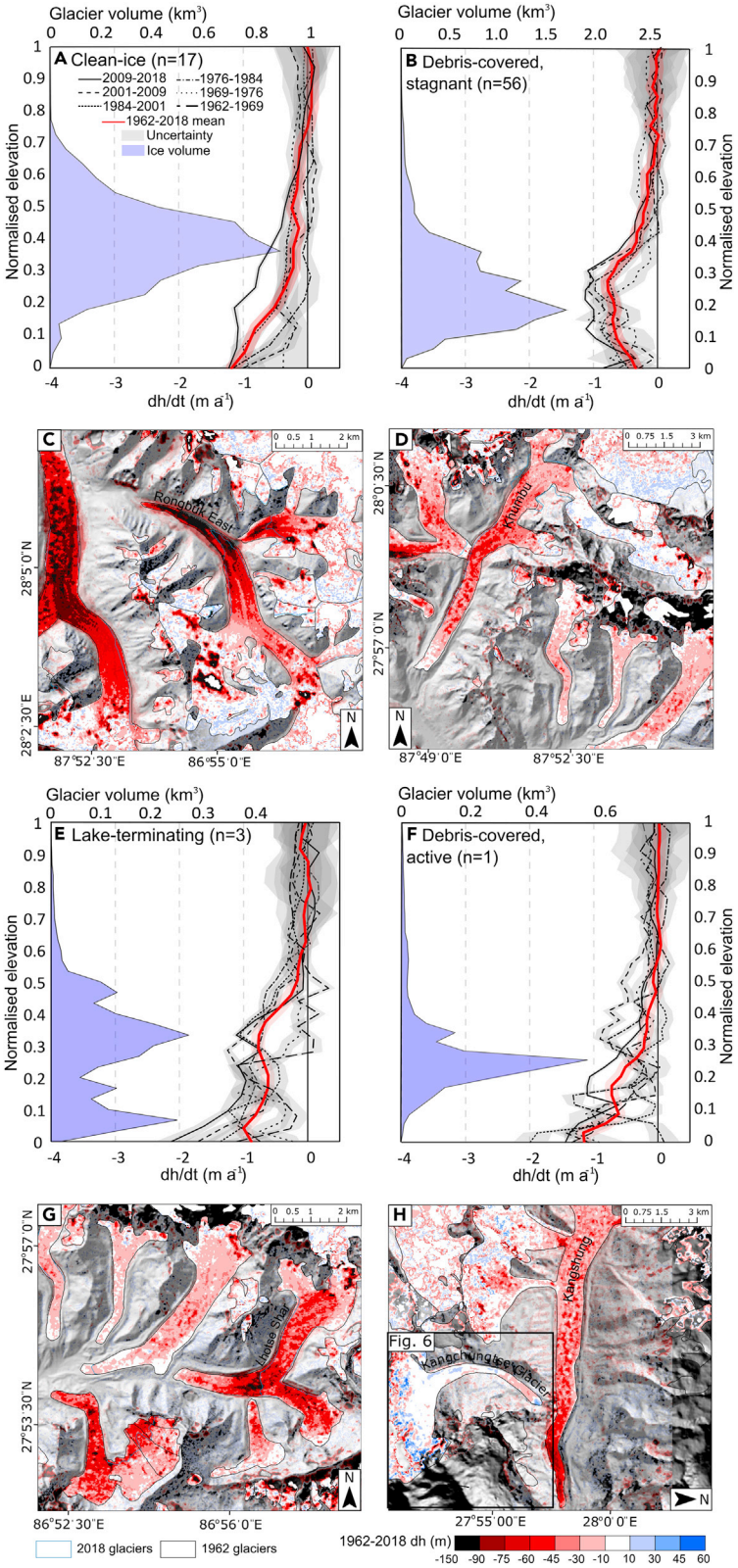

Figure 4. Glacier-Type-Dependent Thinning Regimes in the Mt. Everest Region

The distribution of glacier volume throughout the elevation range of glaciers in the Mt. Everest region (data from Farinotti et al.[29]). Note the variable scaling of the ice volume on the x axis. The evolution of thinning rates for (A) clean-ice, (B) stagnant debris-covered, (E) lake-terminating, and (F) active debris-covered glaciers is shown. Stagnant and active debris-covered glaciers were distinguished with the ITS_LIVE ice surface velocity dataset,[31] whereby substantial (>10 m a^{-1}) ice flow was evident within 1 km of glacier termini. Examples of total glacier surface elevation change (dh) are shown for the clean-ice East Rongbuk Glacier (C), debris-covered and partially stagnant Khumbu Glacier (D), lake-terminating Lhotse Shar/Imja Glacier, (G) and actively flowing, debris-covered Kangshung Glacier (H) over the periods 1962–2017 and 1962–2018.

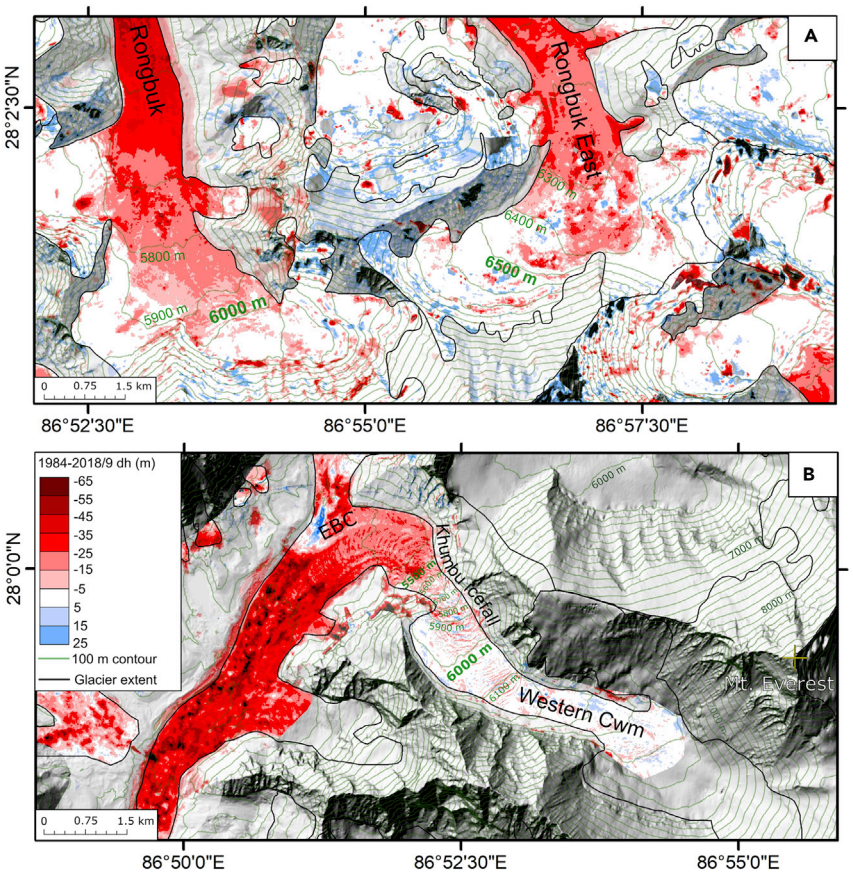

Figure 5. High-Altitude Thinning of Glaciers in the Mt. Everest Region

(A) Difference in the surface elevation between the DEM derived from 1984 aerial photography and the 2018 Cartosat DEM over the upper reaches of Rongbuk and Rongbuk East Glaciers.

(B) Difference in surface elevation between the DEM derived from 1984 aerial photography and the 2019 LiDAR-derived DEM of the Khumbu icefall and the Western Cwm. The background is a hillshade of the composite WorldView DEM (Experimental Procedures). EBC marks Everest Base Camp on Khumbu Glacier.

balance of all glaciers in the Mt. Everest region was −0.23 ± 0.13 meter water equivalent (mwe) a^{-1}. The rate of mass loss increased to −0.31 ± 0.15 mwe a^{-1} between 1976 and 1984 and is now (2009–2018) −0.38 ± 0.13 mwe a^{-1} (Figure 7A). Negative mass balance was pervasive across the region regardless of glacier aspect or terminus type. Barun Glacier displayed the greatest ice loss, the rate of which peaked from 2001 to 2009 at −0.63 ± 0.12 mwe a^{-1}. Khumbu and Rongbuk East Glaciers, which form part of the main climbing routes up Mt. Everest on either side of the main orographic divide, lost ice mass at mean rates of −0.30 ± 0.12 and −0.23 ± 0.12 mwe a^{-1}, respectively, over the full (1962–2018) study period. The contemporary (2009–2018) rates of ice loss from these glaciers (−0.48 ± 0.11 and −0.35 ± 0.11 mwe a^{-1}, respectively) are much higher than their mean rates of ice loss over the full study period.

Glacier-Type-Dependent Variability in Mass Loss

As with other glacierized regions in the Himalaya, glaciers at Mt. Everest display variable surface characteristics and terminus types because of the extensive debris cover, presence of large proglacial lakes, and extreme topography in the region. We divided our mass-balance datasets into categories of different terminus types and levels of debris cover to examine the influence of glacier characteristics on rates of mass loss. We classified glaciers as lake terminating when clear contact was evident between glacier termini and a proglacial lake in our generated orthophotos (n = 3; Lhotse Shar/Imja, Kangshung North, and Hunku Glaciers). We divided our land-terminating glacier mass-balance sample into debris-covered glaciers (n = 57) and clean-ice glaciers (n = 19) on the basis of an 18% debris-coverage threshold.[35] Consistent differences in the rate of mass loss from these different glacier types are evident in our results, particularly in our more contemporary datasets (Figure 7C). Between 1962 and 1969, clean-ice (−0.17 ± 0.11 mwe a^{-1}), debris-covered (−0.25 ± 0.11 mwe a^{-1}), and lake-terminating (−0.22 ± 0.11 mwe a^{-1}) glaciers lost ice at comparable rates. Between 1969 and 1976, rates of ice mass loss from all glaciers increased slightly (Figure 7B), but the range between rates of ice loss from glaciers of different levels of surface cover and terminus types remained small (−0.22 ± 0.11 to −0.29 ± 0.11 mwe a^{-1}). However, since the late 1970s, the rate of ice mass loss from lake-terminating glaciers increased markedly in comparison with that of other glacier types in the Everest region. Between 1976 and 1984, rates of ice mass loss were ~40% higher for lake-terminating glaciers (−0.41 ± 0.14 mwe a^{-1}) than for land-terminating glaciers (−0.30 ± 0.14 mwe a^{-1}). Lake-terminating glaciers lost ice at a rate (−0.51 ± 0.13 mwe a^{-1}) that was ~70% greater than that of land-terminating glaciers (−0.30 ± 0.13 mwe a^{-1}) between 1984 and 2001, at a rate that was ~40% greater than that of land-terminating glaciers from 2001 to 2009 (−0.45 ± 0.12 versus −0.32 ± 0.12 mwe a^{-1}), and at a rate that was 23% greater than that of land-terminating glaciers between 2009 and 2018 (−0.44 ± 0.12 versus −0.38 ± 0.12 mwe a^{-1}; Table S2). Similarly, the rate of ice loss of debris-covered glaciers remained elevated above that of clean-ice glaciers throughout our study period. The greatest difference (~47%) in rates of ice loss from clean-ice and debris-covered glaciers occurred between 1962 and 1969, although rates of ice loss were generally lower in this period. Between the start of the 1970s and 2018, the rate of ice loss of debris-covered glaciers was consistently ~30% higher than that of clean-ice glaciers in the Mt. Everest region.

DISCUSSION

Evolution of Glacier Mass Changes

Glaciers across the Himalaya have been retreating and losing mass for several decades.[6,16,36] The current (2009–2018) rate

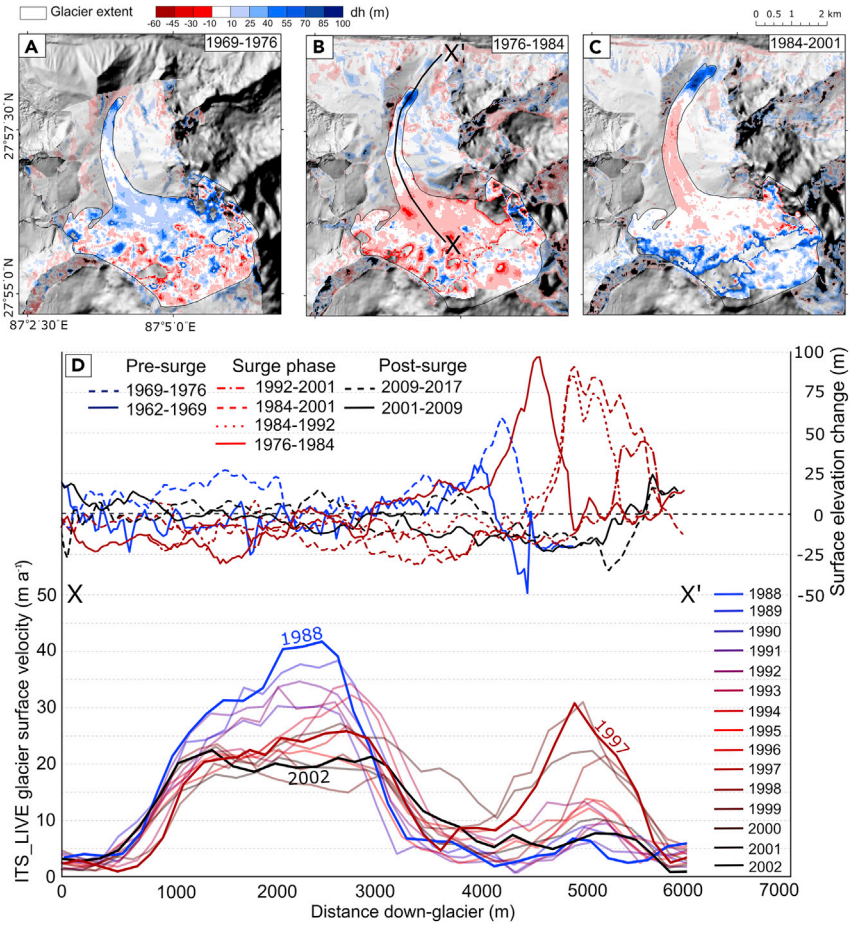

Figure 6. The Surge of Kangchungtse Glacier

Glacier surface elevation from 1969–1976 (A), 1976–1984 (B), and 1984–2001 (C) and along the centerline marked in (B) over each time period (D). Also shown are measurements of glacier surface velocity from Dehecq et al.[33] along the same centerline profiles between 1988 and 2002.

of ice mass loss in the Mt. Everest region (-0.38 ± 0.11 mwe a^{-1}) is comparable with that elsewhere in the Himalaya[14] and is not significantly lower than the global mean rate of glacier mass loss (-0.47 ± 0.20 mwe a^{-1})[37] despite the extreme elevation of the region's glaciers. Our results suggest that ice loss from glaciers in the Mt. Everest region predates even the spy satellite era and that rates of ice loss have consistently increased since the early 1960s (Figure 7A). A general increase in rates of ice loss elsewhere in the Himalaya has been shown across two broad time steps starting in the mid-1970s.[15,16] Our results build on these observations and offer a detailed record of the evolution of glacier mass loss in the central Himalaya.

A time series of temperature measurements compiled from meteorological stations across the Himalaya[38] shows that gradual temperature increases, amounting to an overall increase of ~1°C, occurred on the southern slopes of the central Himalaya, over the eastern Tibetan Plateau, and on the wider Hindu Kush Himalaya throughout the duration of our study period. These meteorological observations suggest a slight increase in temperature (~0.3°C above the 1961–1990 mean) between the mid-1930s and 1950s (prior to our study period), which could have initiated ice loss in the Mt. Everest region.

Reasons for Heterogenous Loss of Ice Mass

Although glacier mass loss has primarily occurred in the Himalaya in response to rising air temperatures,[15] the substantial inter-regional variability in rates of ice loss[6,13,14] suggests that factors other than rising air temperatures are exacerbating rates of ice loss. King et al.[16] examined the impact of factors such as glacier debris cover and proglacial lake development on rates of glacier mass loss elsewhere in the Himalaya, although not in the Mt. Everest region, over two broad study periods between 1974 and 2015. In concurrence with King et al.,[16] our results show that glaciers that have developed large proglacial lakes have lost ice mass at the greatest rate in the Mt. Everest region (Figure 7B) and that glaciers with substantial debris cover have lost ice mass at a comparable, and perhaps slightly increased, rate to that of clean-ice glaciers over multi-decadal time periods (Figure 7B). Further to King et al.,[16] our results show that the elevated rates of mass loss from lake-terminating glaciers could persist for several decades, during which time the rates of glacier terminus retreat and glacier surface velocities could increase.[39,40] After this phase of enhanced flow and ice loss, the rates at which lake-terminating glaciers lose mass diminish to a level comparable to that of land-terminating glaciers (Figure 7C), presumably because their termini retreat to the periphery of their proglacial lake.[41]

An additional consideration that is often not corrected for in the derivation of lake-terminating glacier mass balance is the portion of subaqueous ice that is lost during glacier recession, which is not captured in DEMs that represent the lake surface.[18] This missing ice volume can be captured only by detailed lake bathymetry surveys, which are scarce in the Himalaya. Imja Tsho is the best studied glacial lake in the Mt. Everest region, so we were able to adjust the ice loss for Lhotse Shar/Imja Glacier by using the bathymetry data of Haritashya et al.[42] The addition of the volume of Imja Tsho (78.4×10^6 m^3) to the ice-loss budget of Lhotse Shar/Imja Glacier increases its rate of mass loss from -0.48 ± 0.12 to -0.59 ± 0.12 mwe a^{-1} (a 23% increase) over the period of 1962–2018. Our adjustment for subaqueous ice loss is slightly higher than the 17% increase estimated by Bolch et al.[27] for the same glacier between 1970 and 2007 and most likely reflects the retreat of the glacier into deeper water between the two study periods. Given the scarcity of bathymetric data across the region, estimates of geodetic mass balance for lake-terminating glaciers should clearly be considered minimum estimates, and ice mass loss from this

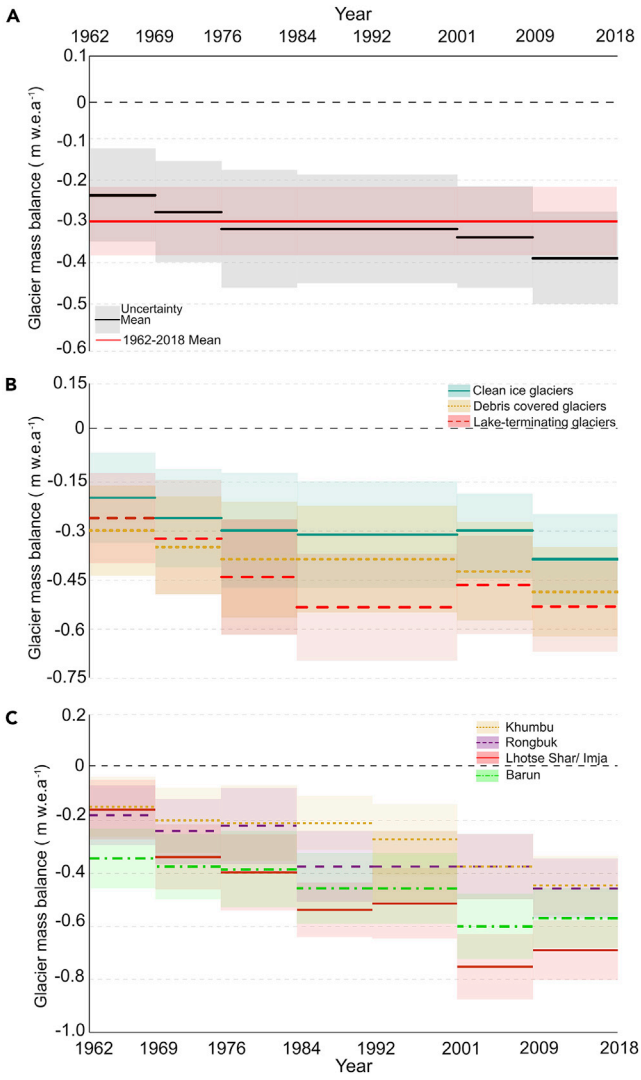

Figure 7. Estimates of Geodetic Glacier Mass Balance over the Mt. Everest Region for Different Time Periods

Estimates of geodetic mass balance for (A) different time periods across the whole region, (B) glaciers of different surface and terminus characteristics, and (C) individual glaciers. The uncertainty associated with estimates of geodetic mass balance for each time period is shown by semi-transparent shading. Note that we do not present region-wide results including the year 1992 because of incomplete coverage for this year and that the y axis is scaled differently for each panel.

type of glacier might be considerably higher than previously reported.

The comparable and perhaps even slightly higher rate of mass loss of debris-covered glaciers than of clean-ice glaciers disagrees with the assertion that the protection of underlying ice by a thick debris layer[43,44] could limit ice loss at the debris-covered-glacier scale. Comparable ice loss has now been measured from debris-covered and clean-ice glaciers over broad spatial[35] and temporal[15,16] scales, and we show that the phenomenon has persisted unchanged for several decades in the central Himalaya. Such findings reinforce the idea that ablation hotspots at the surface of debris-covered glaciers, such as supraglacial ponds and ice cliffs,[45–47] contribute a substantial portion of a glacier's ablation budget and show that their evolution in time and space should be studied in detail. Similarly, the temporal resolution of our data expands on the work of earlier studies[18,23] that used some of the same datasets we examined to reveal ice loss from Mt. Everest. Our results closely match those of Bolch et al.,[27] who also examined Corona imagery, over the 1970–2007 period (Figure S1 and Table S1). Our results incorporating data derived from the 1992 aerial photography survey and 2001 ASTER data suggest slightly higher mass loss over the period across the millennium (-0.34 ± 0.13 mwe a^{-1} from 1992 to 2001) than Nuimura et al.[23] (-0.26 ± 0.13 mwe a^{-1} from 1992 to 2008), although the study periods are not identical and the estimates of mass balance are well within the uncertainty of each study. Our estimates of mass balance compare well with those of other studies that analyzed alternative contemporary datasets (Figure S1 and Table S1).

Glacier Surging in the Central Himalaya

The contrasting thinning and thickening patterns along the length of Kangchungtse Glacier are typical of surge-type glacier behavior, whereby ice mass is redistributed in the down-glacier direction over a relatively short-lived (several years) period of elevated ice flow after what is typically a prolonged period (decades) of ice-mass buildup (the quiescent phase), mainly in their higher reaches, when surface velocities are subdued in comparison with their active surge phase.[48] Despite the length of our time series of observations, we are not able to resolve the length of the quiescent phase of Kangchungtse Glacier, and therefore the duration of its full surge cycle remains unknown. Given the prevalence of ice loss and glacier retreat elsewhere in the region, it is unlikely that the advance and thickening of Kangchungtse Glacier can be attributed to the influence of the local climate on glacier extent. The time series of velocity data provided by the ITS_LIVE dataset (Figure 6) and the terminus advance evident in the orthoimages we generated (Figure S2) suggest that the active phase of the surge cycle of Kangchungtse Glacier occurred between 1976 and 2001. This 25 year active phase is longer than that of most surge-type glaciers found elsewhere in HMA, such as in the Karakoram and Eastern Pamir,[49,50] Tien Shan,[51] the central Tibetan Plateau,[52] and the central Himalaya.[53] The peak active-phase velocities we measured (Figure 6) are also well below those of surge-type glaciers elsewhere in HMA.

Surge-type glaciers predominantly exist in clusters[54] and are prevalent where specific climatic envelopes and glacier attributes allow for surge behavior. Sevestre and Benn[54] highlight the central Himalaya as an area where surge-type glaciers could occur but show no record of glacier surging in the region. Lovell et al.[53] then documented the surge of Sabche Glacier in Manaslu National Park in central Nepal, and our observations of the behavior of Kangchungtse Glacier reinforce Sevestre and Benn's suggestion[54] that glacier surging can occur in the central Himalaya. The limited observations of glacier surging in the central Himalaya could suggest that the region sits on the edge of the climatic envelope suggested by Sevestre and Benn,[54] and long-term warming[15] could make surge-type behavior less likely in the future. In addition to climatic conditions and glacier

geometry attributes, basal topography and geology can promote surging. Lovell et al.[53] suggested that the position of an overdeepening and confining valley geometry could control the surging behavior of Sabche Glacier, and the spatially restricted nature of enhanced ice flow during the early part of the active phase of the surge of Kangchungtse Glacier (Figure 6D) could hint at the impact of glacier bed and valley topography on glacier surging in the Mt. Everest region. Surge-type glacier behavior might therefore not be widespread elsewhere in the central Himalaya unless specific topographic conditions promote unstable glacier flow.

Future Glacier Evolution and Its Implications

Our spatially and temporally comprehensive observations of glacier mass change in the Mt. Everest region over the last six decades show the impact of climate change on the cryosphere in the central Himalaya. We have documented how the rate of mass loss has increased from the glaciers around Mt. Everest since the 1960s. The increase in mass loss has occurred because thinning rates are accelerating in glacier ablation zones, large proglacial lakes are expanding, and ice losses are occurring at higher elevation ranges. Given the projected temperature increases under all representative concentration pathway (RCP) scenarios in the central Himalaya,[55] which might be amplified at higher altitudes,[56] it seems highly likely that rates of ice loss will further increase from glaciers in the Mt. Everest region in the coming decades. Repeat observations of high-altitude glacier change, specifically at and above current glacier equilibrium-line altitudes, will become increasingly important in understanding glacier response to even more substantial climatic forcing. Remotely sensed imagery of moderate spatial or radiometric resolution fails to reliably capture surface conditions in glacier accumulation zones, but we have shown the suitability of high-altitude LiDAR data in the derivation of rates of glacier surface elevation change at high altitude. The repeated acquisition of such data would allow for the accurate assessment of high-altitude glacier change, which is currently only loosely constrained.

Amplified glacier mass loss will affect communities downstream through increased pressure on water resources and through the development of glacier hazards during deglaciation. Glacial lake outburst floods (GLOFs) have occurred historically[57] and recently[58,59] in the Himalaya, and glacier recession will fuel the expansion of current and the formation of new glacial lakes. The expansion of lakes up valley, toward terrain more prone to avalanching and mass movements,[60] could increase the likelihood of GLOF occurrence, although GLOF events have shown no significant increase in the region in recent decades.[59] Greater glacier mass loss will also affect the much relied-upon seasonality of both local[61] and regional[7] river flow, as well as limit the longevity of Himalayan glaciers as a sustainable component of the Asian water tower. Within the Khumbu Valley, glacial melt provides ~65% of the water used by the local community during the pre-monsoon dry season,[61] and continued glacier melt and snowpack decline will clearly increase water stress within the Mt. Everest region before the initiation of the monsoon each year. Further afield, the contribution of glacial meltwater originating in the Himalaya to the flow of some of Asia's largest rivers, such as the Ganges, Indus, and Brahmaputra, will become increasingly important toward the end of the 21st century,[7,8] particularly during years of drought.[4] Huss and Hock[7] and Rounce et al.[8] suggest substantial shifts in the annual timing of peak glacier runoff under different RCPs for these rivers, which, in combination with a high population density downstream, will increase water stress once glacier meltwater yields begin to decline. The continued assessment of glacier change in the Mt. Everest region, and Himalaya as a whole, is clearly vital if we are to understand—and both local and distal communities are to adapt to—the impacts of climate change on the region. Ultimately, our time series of geodetic observations provides a benchmark dataset against which physically based glacier models should be calibrated before they are used for predicting such future glacier behavior and meltwater yield in decades to come.

EXPERIMENTAL PROCEDURES

Resource Availability

Lead Contact

Further information and requests for resources should be directed to and will be fulfilled by the Lead Contact, Owen King (ogak1@st-andrews.ac.uk).

Materials Availability

The DEM difference data and glacier outlines generated for this study are available through PURE (https://doi.org/10.17630/b453ff7d-7cd0-45cf-b31e-50847227b60c) or upon request from the Lead Contact.

Data and Code Availability

The datasets generated during this study are available in PURE, the official data repository of the University of St Andrews (https://doi.org/10.17630/b453ff7d-7cd0-45cf-b31e-50847227b60c).

Data Acquisition

We have assembled a time series of geodetic data spanning 56 years over Mt. Everest and its surrounding glaciated valleys. Our study area extends that of the 1988 National Geographic Map of Mt. Everest, which covers an area of 945 km^2. The map area covers 212 glaciers, of which we derive estimates of elevation change and geodetic mass balance for 79 (88% of the total glacier area), considering a minimum size threshold of 1 km^2. The 1988 National Geographic map area only partially covers Kangshung and Barun Glaciers to the east of Mt. Everest (Figure 1). In these two cases, we used complementary PlanetScope imagery to extend the study area's boundary slightly to increase coverage of the glacier area (Table 1). The geodetic time series is based on DEMs generated from declassified spy satellite imagery acquired by Corona KH-4 (1962), Corona KH-4B (1969), and Hexagon KH-9 (1976) satellites; aerial photograph surveys (1984 and 1992); and satellite imagery acquired by contemporary sensors such as ASTER (2001), Cartosat (2009), PlanetScope (2017), and Cartosat 2 (2018), as well as a high-altitude LiDAR survey conducted over Khumbu Glacier in 2019.[28]

We referred to a master DEM and associated orthoimage to fix the geolocation of all DEMs in our time series. This control dataset is a composite generated from WorldView-1 and -2 imagery (0.5 m ground resolution) acquired between January 31, 2012, and February 28, 2017, from which ground control points (>15 for all time periods) were collected during DEM generation for each time period. Any remnant shifts between DEMs from different epochs were removed by a three-step DEM co-registration approach.[62]

We derived glacier surface elevation change (dh) by differencing the DEMs from each time period. We considered values outside of the range ±150 m in elevation change data to be outliers and applied a secondary filtering step by using an elevation-dependent sigmoid function[63] to remove anomalous data caused by low image quality. We filled the resulting data gaps (Table S3) in two stages. First, for small data gaps, we used a mean value from surrounding cells within a 4 × 4 window. Larger data gaps were filled with values of the median elevation change within the closest 100 m elevation band.[64] To estimate geodetic glacier mass balance, we converted elevation change to ice volume change by considering the pixel size of dh grids (30 m) and then to ice mass change by using an average ice density estimate of 850 ± 60 kg m^3.[65] Estimates

Table 1. Data Sources Used for Generating the Geodetic Time Series of Glacier Surface Elevation Change

Sensor and Scene ID	Date of Acquisition	Image Resolution	Area Covered
Corona KH-4	December 15, 1962	7.6 m	whole region
Corona KH-4A	December 18, 1969	5.2 m	whole region
Corona KH-4B	November 20, 1970	4 m	whole region
Hexagon KH-9	January 3, 1976	7.6 m	whole region
Aerial photography 1984 (Washburn set) Wild RC-10	December 20, 1984	0.5 m	whole region
Aerial photography 1992 (Nepali set) Wild RC-30	November 19, 1992	2.5 m	south of orographic divide
ASTER	December 8, 2001	15 m	whole region
Cartsosat	October 29, 2009	2.5 m	whole region
PlanetScope	November 7–19, 2017	3–4 m	Kangshung Glacier
Cartosat 2	December 15, 2018	2.5 m	whole region
LiDAR	May 2019	–	Khumbu Glacier

of mass balance were derived over glacier areas manually modified with ortho images from each epoch as a reference and the RGI V 6.0 as a baseline dataset. We also used our dh data to modify glacier outlines in areas where debris-covered ice could have been mistaken for off-glacier terrain but where ice thinning was still occurring, for example, at the terminus of Khumbu Glacier.

The acquisition dates of all the images we used in DEM generation—aside from the 1976 Hexagon imagery, which was acquired toward the end of the winter season—were from the same season (Table 1). We therefore consider that the glacier surfaces represented by the 1976 Hexagon DEM are actually more representative of the end-of-ablation-season surface from 1975 and use this date in our calculations of elevation change. We do not consider seasonality corrections for other datasets.

The differencing of DEMs derived from optical imagery, such as our time series, over the lake-terminating potion of a glacier only yields elevation change data between the lake level and the surface of the glacier; this potentially large amount of ice below the water line is not accounted for in the mass-loss budget of the glacier. Considering the full depth of Imja Tsho at the date of the survey (2015) and the area of the lake at the different epochs within our time series, we used the bathymetric data of Haritashya et al.[42] to correct the mass-loss budget of Lhotse Shar/Imja Glacier. The magnitude of the adjustment of geodetic mass-balance estimates ranges from 0.02 to 0.16 mwe a^{-1} for different time periods (Figure S3) and depends largely on the depth profile of Imja Tsho in the up-glacier direction.

Estimation of Uncertainty

We consider the uncertainty associated with estimates of geodetic mass balance to be a combination of the uncertainty associated with elevation change ($(E_{\Delta h})$), the uncertainty associated with a changing glacier area ($E_{\Delta \boldsymbol{A}}$), the uncertainty associated with volume-to-mass conversion ($E_{\Delta m}$), and the influence of spatially nonuniform glacier area on the distribution of uncertainty.[66,67] We estimate ($(E_{\Delta h})$) through

$$E_{\Delta h} = \frac{\sigma_{\text{stable}}}{\sqrt{N}}, \qquad \text{(Equation 1)}$$

where N is the effective number of observations and σ_{stable} is the standard deviation of the mean elevation change of off-glacier stable terrain. N is calculated through

$$N = \frac{N_{\text{tot}}.PS}{2d}, \qquad \text{(Equation 2)}$$

where N_{tot} is the total number of dh data points, PS is the pixel size of the dh grids (30 m), and d is the distance of spatial autocorrelation. We used an autocorrelation value (d) of 600 m here (20 pixels),[27] although this value most likely varies between datasets. The uncertainty associated with $E_{\Delta m}$ is taken as 7% of the mass-loss estimate,[65] and the uncertainty associated with a changing glacier area[67] is taken to be

$$E_{\Delta A} = \left(\frac{\delta \boldsymbol{A}}{\mathrm{A}}\right)^2. \qquad \text{(Equation 3)}$$

$E_{\Delta h}$, $E_{\Delta m}$, and $E_{\Delta \boldsymbol{A}}$ are summed quadratically:

$$\sigma_{\Delta m} = \sqrt{E_{\Delta h}^2 + E_{\Delta m} + E_{\Delta A}^2}. \qquad \text{(Equation 4)}$$

$\sigma_{\Delta m}$ is weighted depending on glacier hypsometry (Figure S4) to better represent the spatial heterogeneity of uncertainty, where higher uncertainty is commonly associated with steeper terrain high in glacier accumulation zones.[66]

SUPPLEMENTAL INFORMATION

Supplemental Information can be found online at https://doi.org/10.1016/j.oneear.2020.10.019.

ACKNOWLEDGMENTS

We thank the National Geographic and Rolex Perpetual Planet Partnership for its invaluable support. The 2019 helicopter scanning was conducted in partnership with the National Geographic Society, Rolex, and Tribhuvan University with approval from all relevant agencies of the government of Nepal. We also wish to thank the communities of the Khumbu Region and Shangri-La Nepal Trek for supporting that endeavor. We thank Ram Raj Rijal and Dhananjay Regmi for their sharing of 1992 aerial photographs. We are grateful for the assistance of BSF Swissphoto in providing and scanning the 1984 aerial photographs. We are also grateful to three anonymous reviewers for their carefully considered comments, which helped improve the manuscript substantially.

AUTHOR CONTRIBUTIONS

Conceptualization, O.K., T.B., and A.B.; Methodology, O.K., T.B., S. Ghuffar, and A.B.; Software, O.K. and A.B.; Resources, A.T.; Data Curation, O.K., A.B., A.T., S. Guilford, and S. Ghuffar; Writing – Original Draft, O.K.; Writing – Review & Editing, O.K., T.B., A.B., A.C.E., and A.T.; Supervision, T.B.; Funding Acquisition, A.C.E. and A.T.

DECLARATION OF INTERESTS

The authors declare no competing interests.

Received: August 7, 2020
Revised: October 16, 2020
Accepted: October 28, 2020
Published: November 20, 2020

REFERENCES

1. Sharma, E., Molden, D., Rahman, A., Khatiwada, Y.R., Zhang, L., Singh, S.P., Yao, T., and Wester, P. (2019). Introduction to the Hindu Kush Himalaya Assessment. In The Hindu Kush Himalaya Assessment: Mountains, Climate Change, Sustainability and People, P. Wester, A. Mishra, A. Mukherji, and A.B. Shrestha, eds. (Springer International Publishing), pp. 1–16.
2. Immerzeel, W.W., Lutz, A.F., Andrade, M., Bahl, A., Biemans, H., Bolch, T., Hyde, S., Brumby, S., Davies, B.J., Elmore, A.C., et al. (2019). Importance and vulnerability of the world's water towers. Nature *577*, 364–369.
3. Immerzeel, W.W., and Bierkens, M.F.P. (2012). Asia's water balance. Nat. Geosci. *5*, 841–842.
4. Pritchard, H.D. (2019). Asia's shrinking glaciers protect large populations from drought stress. Nature *569*, 649–654.
5. Intergovernmental Panel on Climate Change (2014). Part B: regional aspects. In Climate Change 2014: Impacts, Adaptation, and Vulnerability. Contribution of Working Group II to the Fifth Assessment Report of the Intergovernmental Panel on Climate Change, V.R. Barros, C.B. Field, D.J. Dokken, M.D. Mastrandrea, K.J. Mach, T.E. Bilir, M. Chatterjee, K.L. Ebi, Y.O. Estrada, and R.C. Genova, et al., eds. (Cambridge University Press). https://www.ipcc.ch/report/ar5/wg2/.
6. Bolch, T., Shea, J.M., Liu, S., Azam, F.M., Gao, Y., Gruber, S., Immerzeel, W.W., Kulkarni, A., Li, H., Tahir, A.A., et al. (2019). Status and change of the cryosphere in the extended Hindu Kush Himalaya region. In The Hindu Kush Himalaya Assessment: Mountains, Climate Change, Sustainability and People, P. Wester, A. Mishra, A. Mukherji, and A.B. Shrestha, eds. (Springer International Publishing), pp. 209–255.
7. Huss, M., and Hock, R. (2018). Global-scale hydrological response to future glacier mass loss. Nat. Clim. Chang. *8*, 135–140.
8. Rounce, D.R., Hock, R., and Shean, D. (2020). Glacier mass change in high mountain Asia through 2100 using the open-source python glacier evolution model (PyGEM). Front. Earth Sci. *7*, 331.
9. Bolch, T., Kulkarni, A., Kääb, A., Huggel, C., Paul, F., Cogley, J., Frey, H., Kargel, J., Fujita, K., Scheel, M., et al. (2012). The state and fate of Himalayan glaciers. Science *336*, 310–314.
10. Yao, T., Thompson, L., Yang, W., Yu, W., Gao, Y., Guo, X., Yang, X., Duan, K., Zhao, H., Xu, B., et al. (2012). Different glacier status with atmospheric circulations in Tibetan Plateau and surroundings. Nat. Clim. Chang. *2*, 663–667.
11. World Glacier Monitoring Service (2019). Fluctuations of Glaciers Database. https://doi.org/10.5904/wgms-fog-2019-12.
12. Gardner, A.S., Moholdt, G., Cogley, J.G., Wouters, B., Arendt, A.A., Wahr, J., Berthier, E., Hock, R., Pfeffer, W.T., Kaser, G., et al. (2013). A reconciled estimate of glacier contributions to sea level rise: 2003 to 2009. Science *340*, 852–857.
13. Brun, F., Berthier, E., Wagnon, P., Kääb, A., and Teichler, D. (2017). A spatially resolved estimate of high mountain Asia glacier mass balances from 2000 to 2016. Nat. Geosci. *10*, 668–673.
14. Shean, D.E., Bhushan, S., Montesano, P., Rounce, D.R., Arendt, A., and Osmanoglu, B. (2020). A systematic, regional assessment of high-mountain Asia glacier mass balance. Front. Earth Sci. *7*, https://doi.org/10.3389/feart.2019.00363.
15. Maurer, J.M., Schaefer, J.M., Rupper, S., and Corley, A. (2019). Acceleration of ice loss across the Himalayas over the past 40 years. Sci. Adv. *5*, 6.
16. King, O., Bhattacharya, A., Bhambri, R., and Bolch, T. (2019). Glacial lakes exacerbate Himalayan glacier mass loss. Sci. Rep. *9*, 18145.
17. Zhou, Y., Li, Z., Li, J., Zhao, R., and Ding, X. (2018). Glacier mass balance in the Qinghai–Tibet Plateau and its surroundings from the mid-1970s to 2000 based on Hexagon KH-9 and SRTM DEMs. Remote Sens. Environ. *210*, 96–112.
18. Bolch, T., Buchroithner, M., Pieczonka, T., and Kunert, A. (2008). Planimetric and volumetric glacier changes in the Khumbu Himal, Nepal, since 1962 using Corona, Landsat TM and ASTER data. J. Glaciol. *54*, 592–600.
19. Mukherjee, K., Bhattacharya, A., Pieczonka, T., Ghosh, S., and Bolch, T. (2018). Glacier mass budget and climate reanalysis data indicate a climatic shift around 2000 in Lahaul-Spiti, western Himalaya. Clim. Change *148*, 219–233.
20. Schneider, E. (1957). Mahalangur-Himal. Begleitworte zur Alpenvereinskarte des Everestgebietes 1:25.000. Jhb. des Österr. Alpenvereins *82*, 5–12.
21. Washburn, B. (1989). Mapping Mount Everest. Bull. Am. Acad. Arts Sci. *42*, 29–44.
22. Hahn, M., Baral, T.N., and Sharma, R.K. (2002). A study on digital orthophoto generation of Mount Everest region. In Proceedings of the 23rd Asian Conference on Remote Sensing (Asian Association on Remote Sensing). https://a-a-r-s.org/proceeding/ACRS2002/Papers/PHG02-3.htm.
23. Nuimura, T., Fujita, K., Yamaguchi, S., and Sharma, R.R. (2012). Elevation changes of glaciers revealed by multitemporal digital elevation models calibrated by GPS survey in the Khumbu region, Nepal Himalaya, 1992–2008. J. Glaciol. *58*, 648–656.
24. Ye, Q., Bolch, T., Naruse, R., Wang, Y., Zong, J., Wang, Z., Zhao, R., Yang, D., and Kang, S. (2015). Glacier mass changes in Rongbuk catchment on Mt. Qomolangma from 1974 to 2006 based on topographic maps and ALOS PRISM data. J. Hydrol. (Amst.) *530*, 273–280.
25. King, O., Quincey, D.J., Carrivick, J.L., and Rowan, A.V. (2017). Spatial variability in mass loss of glaciers in the Everest region, central Himalayas, between 2000 and 2015. Cryosphere *11*, 407–426.
26. Li, G., Lin, H., and Ye, Q. (2018). Heterogeneous decadal glacier downwasting at the Mt. Everest (Qomolangma) from 2000 to 2012 based on multi-baseline bistatic SAR interferometry. Remote Sens. Environ. *206*, 336–349.
27. Bolch, T., Pieczonka, T., and Benn, D.I. (2011). Multi-decadal mass loss of glaciers in the Everest area (Nepal Himalaya) derived from stereo imagery. Cryosphere *5*, 349–358.
28. Tait, A., Jaskolski, C., Broad, K., Millbern, C., Chapple, R., Carter, P., Grasiemko, M., Guilford, S., Elmore, A.C., Dangol, S., et al. (2020). High Resolution Lidar Data of Khumbu Glacier (Dryad). https://doi.org/10.5061/dryad.73n5tb2vx.
29. Farinotti, D., Huss, M., Furst, J.J., Landmann, J., Machguth, H., Maussion, F., and Pandit, A. (2019). A consensus estimate for the ice thickness distribution of all glaciers on Earth. Nat. Geosci. *12*, 168–173.
30. RGI Consortium (2017). Randolph Glacier Inventory – A Dataset of Global Glacier Outlines, Version 6.0: Technical Report, Global Land Ice Measurements from Space. https://doi.org/10.7265/N5-RGI-60.
31. Rowan, A.V., Egholm, D.L., Quincey, D.J., and Glasser, N.F. (2015). Modelling the feedbacks between mass balance, ice flow and de-bris transport to predict the response to climate change of debris-covered glaciers in the Himalaya. Earth Planet. Sci. Lett. *430*, 427–438.
32. Pieczonka, T., Bolch, T., Kröhnert, M., Peters, J., and Liu, S. (2018). Glacier branch lines and glacier ice thickness estimation for debris-covered glaciers in the Central Tien Shan. J. Glaciol. *64*, 835–849.
33. Dehecq, A., Gourmelen, N., Gardner, A.S., Brun, F., Goldberg, D., Nienow, P.W., Berthier, E., Vincent, C., Wagnon, P., and Trouve, E. (2019). Twenty-first century glacier slowdown driven by mass loss in High Mountain Asia. Nat. Geosci. *12*, 22–27.
34. Gardner, A.S., Fahnestock, M.A., and Scambos, T.A. (2020). ITS_LIVE Regional Glacier and Ice Sheet Surface Velocities. Data archived at the National Snow and Ice Data Center. https://doi.org/10.5067/6II6VW8LLWJ7.
35. Brun, F., Wagnon, P., Berthier, E., Jomelli, V., Maharjan, S.B., Shrestha, F., and Kraaijenbrink, P.D.A. (2019). Heterogeneous influence of glacier morphology on the mass balance variability in high mountain Asia. J. Geophys. Res. Surface *124*, 1–15.
36. Azam, M.F., Wagnon, P., Berthier, E., Vincent, C., Fujita, K., and Kargel, J.S. (2018). Review of the status and mass changes of Himalayan-Karakoram glaciers. J. Glaciol. *64*, 61–74.

37. Zemp, M., Huss, M., Thibert, E., Eckert, N., McNabb, R., Huber, J., and Cogley, J.G. (2019). Global glacier mass changes and their contributions to sea-level rise from 1961 to 2016. Nature *568*, 382–386.

38. Ren, Y.Y., Ren, G.Y., Sun, X.B., Shrestha, A.B., You, Q.L., Zhan, Y.J., Rajbhandari, R., Zhang, P.F., and Wen, K.M. (2017). Observed changes in surface air temperature and precipitation in the Hindu Kush Himalayan region over the last 100-plus years. Adv. Clim. Chang. Res. *8*, 148–156.

39. Watson, C.S., Kargel, J.S., Shugar, D.H., Haritashya, U.K., Schiassi, E., and Furfaro, R. (2020). Mass loss from calving in Himalayan proglacial lakes. Front. Earth Sci. *7*, 342.

40. Liu, Q., Mayer, C., Wang, X., Nie, Y., Wu, K., Wei, J., and Liu, S. (2020). Interannual flow dynamics driven by frontal retreat of a lake-terminating glacier in the Chinese Central Himalaya. Earth Planet. Sci. Lett. *546*, 116450.

41. Zhang, G., Bolch, T., Allen, S., Linsbauer, A., Chen, W., and Wang, W. (2019). Glacial lake evolution and glacier–lake interactions in the Poiqu River basin, central Himalaya, 1964–2017. J. Glaciol. *65*, 347–365.

42. Haritashya, U.K., Kargel, J.S., Shugar, D.H., Leonard, G.J., Strattman, K., Watson, C.S., Shean, D., Harrison, S., Mandli, K.T., and Regmi, D. (2018). Evolution and controls of large glacial lakes in the Nepal Himalaya. Remote Sens. *10*, 798.

43. Østrem, G. (1959). Ice melting under a thin layer of moraine, and the existence of ice cores in moraine ridges. Geogr. Ann. *41*, 228–230.

44. Nicholson, L., and Benn, D.I. (2006). Calculating ice melt beneath a debris layer using meteorological data. J. Glaciol. *52*, 463–470.

45. Buri, P., Miles, E.S., Steiner, J.F., Immerzeel, W.W., Wagnon, P., and Pellicciotti, F. (2016). A physically based 3-D model of ice cliff evolution over debris-covered glaciers. J. Geophys. Res. *121*, 2471–2493.

46. Sakai, A., Nishimura, K., Kadota, T., and Takeuchi, N. (2009). Onset of calving at supraglacial lakes on debris-covered glaciers of the Nepal Himalayas. J. Glaciol. *55*, 909–917.

47. Thompson, S., Benn, D.I., Mertes, J., and Luckman, A. (2016). Stagnation and mass loss on a Himalayan debris-covered glacier: processes, patterns and rates. J. Glaciol. *62*, 467–485.

48. Murray, T., Strozzi, T., Luckman, A., Jiskoot, H., and Christakos, P. (2003). Is there a single surge mechanism? Contrasts in dynamics between glacier surges in Svalbard and other regions. J. Geophys. Res. *108*, 2237.

49. Bhambri, R., Hewitt, K., Kawishwar, P., and Pratap, B. (2019). Surge-type and surge-modified glaciers in the Karakoram. Sci. Rep. *7*, 15391.

50. Lv, M., Guo, H., Lu, X., Liu, G., Yan, S., Ruan, Z., Ding, Y., and Quincey, D.J. (2019). Characterizing the behaviour of surge- and non-surge-type glaciers in the Kingata Mountains, eastern Pamir, from 1999 to 2016. Cryosphere *13*, 219–236.

51. Mukherjee, K., Bolch, T., Goerlich, F., Kutuzov, S., Osmonov, A., Pieczonka, T., and Shesterova, I. (2017). Surge-type glaciers in the Tien Shan (Central Asia). Arct. Antarct. Alp. Res. *49*, 147–171.

52. Xu, J., Shangguan, D., and Wang, J. (2018). Three-dimensional glacier changes in Geladandong Peak region in the central Tibetan plateau. Water *10*, 1749, https://doi.org/10.3390/w10121749.

53. Lovell, A.M., Carr, J.R., and Stokes, C.R. (2018). Topographic controls on the surging behaviour of Sabche Glacier, Nepal (1967 to 2017). Remote Sens. Environ. *210*, 434–443.

54. Sevestre, H., and Benn, D.I. (2015). Climatic and geometric controls on the global distribution of surge-type glaciers: implications for a unifying model of surging. J. Glaciol. *61*, 646–662.

55. Kraaijenbrink, P.D.A., Bierkens, M.F.P., Lutz, A.F., and Immerzeel, W.W. (2019). Impact of a global temperature rise of 1.5 degrees Celsius on Asia's glaciers. Nature *549*, 257–260.

56. Mountain Research Initiative EDW Working Group (2015). Elevation-dependent warming in mountain regions of the world. Nat. Clim. Chang. *5*, 424–430.

57. Carrivick, J.L., and Tweed, F.S. (2016). A global assessment of the societal impacts of glacier outburst floods. Global Planet. Change *144*, 1–16.

58. Nie, Y., Liu, Q., Wang, J., Zhang, Y., Sheng, Y., and Liu, S. (2018). An inventory of historical glacial lake outburst floods in the Himalayas based on remote sensing observations and geomorphological analysis. Geomorphology *308*, 91–106.

59. Veh, G., Korup, O., von Specht, S., Roessner, S., and Walz, A. (2019). Unchanged frequency of moraine-dammed glacial lake outburst floods in the Himalaya. Nat. Clim. Chang. *9*, 379–383.

60. Lala, J.M., Rounce, D.R., and McKinney, D.C. (2018). Modeling the glacial lake outburst flood process chain in the Nepal Himalaya: reassessing Imja Tsho's hazard. Hydrol. Earth Syst. Sci. *22*, 3721–3737.

61. Wood, L.R., Neumann, K., Nicholson, K.N., Bird, B.W., Dowling, C.B., and Sharma, S. (2020). Melting Himalayan glaciers threaten domestic water resources in the Mount Everest Region, Nepal. Front. Earth. Sci. *8*, https://doi.org/10.3389/feart.2020.00128.

62. Nuth, C., and Kääb, A. (2011). Co-registration and bias corrections of satellite elevation data sets for quantifying glacier thickness change. Cryosphere *5*, 271–290.

63. Pieczonka, T., and Bolch, T. (2015). Region-wide glacier mass budgets and area changes for the Central Tien Shan between ~1975 and 1999 using Hexagon KH-9 imagery. Global Planet. Change *128*, 1–13.

64. McNabb, R., Nuth, C., Kääb, A., and Girod, L. (2019). Sensitivity of glacier volume change estimation to DEM void interpolation. Cryosphere *13*, 895–910, https://doi.org/10.5194/tc-13-895-2019.

65. Huss, M. (2013). Density assumptions for converting geodetic glacier volume change to mass change. Cryosphere *7*, 877–887.

66. Ragettli, S., Bolch, T., and Pellicciotti, F. (2016). Heterogeneous glacier thinning patterns over the last 40 years in Langtang Himal, Nepal. Cryosphere *10*, 2075–2097.

67. Malz, P., Meier, W., Casassa, G., Jana, R., Skvarca, P., and Braun, M.H. (2018). Elevation and mass changes of the Southern Patagonia icefield derived from TanDEM-X and SRTM data. Remote Sens. *10*, 188.